Research Square

Preprints are preliminary reports that have not undergone peer review.
They should not be considered conclusive, used to inform clinical practice,
or referenced by the media as validated information.

Interfacial Hydroxide Engineering of Mxene for High Performance Electrochemical Energy Storage

Ragavi M

regavijammu6598@gmail.com

Kongu Engineering College in

Geetha A

Kongu Engineering College in

Research Article

Keywords: MXene, Magnesium hydroxide, Supercapacitors, Electrochemical energy storage, Interfacial engineering, Mesoporous materials

Posted Date: November 23rd, 2026

DOI: https://doi.org/10.21203/rs.3.rs-11388056/v1

License: This work is licensed under a Creative Commons Attribution 4.0 International License.
Read Full License

Additional Declarations: No competing interests reported.

INTERFACIAL HYDROXIDE ENGINEERING OF MXENE FOR HIGH PERFORMANCE ELECTROCHEMICAL ENERGY STORAGE

A.Geetha[1] & M.Ragavi[1*]

*[1*1] Center for Environmental Research, Department of Chemistry, Kongu Engineering College, Perundurai, Erode – 638060*

Corresponding Mail id - ragavijummu6598@gmail.com

Abstract

The layered structure and rich surface chemistry of MXene-based materials combined with their excellent electrical conductivity make them attractive candidates for high-performance supercapacitor electrodes. But the electrochemical activity of a pristine MXene is limited by the restacking of nanosheets, which decreases accessible surface area and impedes the flow of ions into the material. In this work, the electrochemical properties of MXene electrodes were improved by successfully synthesizing a composite of MXene and $Mg(OH)_2$ using an interfacial hydroxide engineering approach of hydrofluoric acid etching and magnesium hydroxide deposition. The prepared composite was systematically characterized in terms of its structural, surface and electrochemical properties through X-ray diffraction (XRD), X-ray photoelectron spectroscopy (XPS), Brunauer–Emmett–Teller (BET) analysis, cyclic voltammetry (CV), electrochemical impedance spectroscopy (EIS) and galvanostatic charge–discharge (GCD) measurements. The successful preparation of the MXene-$Mg(OH)_2$ composite and confirmation of the presence of Mg–OH functional groups were verified using the XRD and XPS analyses. The S-adsorption study revealed that the specific surface area increased from 26.8 to 58.6 m^2 g^{-1}, pore volume rose from 0.112 to 0.218 cm3 g^{-1}, and the average pore diameter increased from 8.4 to 12.7 nm, which indicated the effect of suppressing MXene restacking and developing a mesoporous structure. Electrochemical studies revealed better capacitive behaviour, better charge-transfer characteristics, and faster ion diffusion when the scan rate was varied from 5 to 100 mV s^{-1}. The synergistic effect of conductive MXene nanosheets and pseudocapacitive $Mg(OH)_2$ resulted in enhanced electrochemical activity and structural stability, which indicates that the composite can be considered as an efficient electrode material for next-generation supercapacitor applications.

keywords: MXene; Magnesium hydroxide; Supercapacitors; Electrochemical energy storage; Interfacial engineering; Mesoporous materials.

Graphical Abstract:

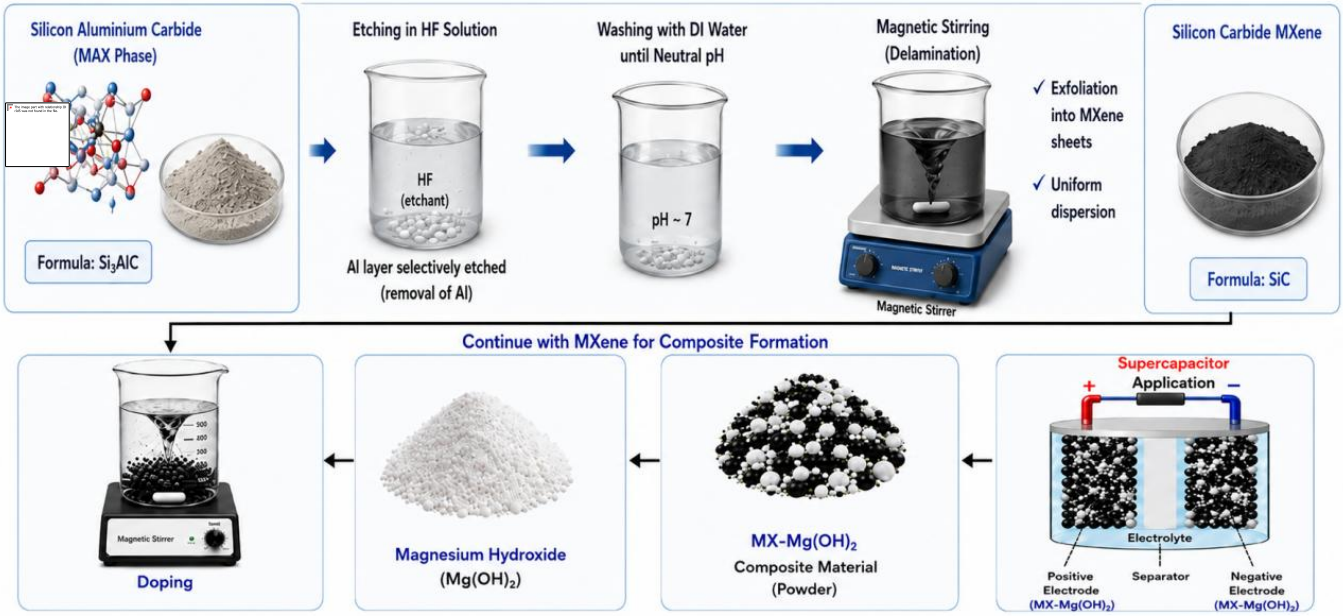

Abbreviation

MAX	-	$M_{n+1}AX_n$ Phase
MXene	-	Two-dimensional Transition Metal Carbide/Nitride
SiC	-	Silicon Carbide
$Mg(OH)_2$	-	Magnesium Hydroxide
HF	-	Hydrofluoric Acid
DI Water	-	Deionized Water
KOH	-	Potassium Hydroxide
EDLC	-	Electrical Double-Layer Capacitance
Rct	-	Charge Transfer Resistance
Zr	-	Real Impedance
Zi	-	Imaginary Impedance
mV s^{-1}	-	Millivolts per Second
µA	-	Microampere
F g^{-1}	-	Farads per Gram
m^2 g^{-1}	-	Square Metres per Gram
cm^3 g^{-1}	-	Cubic Centimetres per Gram
nm	-	Nanometre
eV	-	Electron Volt
Cu-Kα	-	Copper K-alpha Radiation
Si–C	-	Silicon–Carbon Bond

Si–O - Silicon–Oxygen Bond

C–C - Carbon–Carbon Bond

C–O - Carbon–Oxygen Bond

Mg^{2+} - Magnesium Ion

1.INTRODUCTION

The increasing energy demand in the world and the adoption of sustainable energy systems have increased the necessity to have efficient energy storage technologies. Supercapacitors have become of particular interest among the existing energy storage devices and have been studied because of their high power density, long cycle life and rapid charge discharge compared to the traditional batteries [1–3]. Nevertheless, their comparatively low energy density is a severe limitation that requires the creation of high-performance electrode materials with improved electrochemical functions [4,5]. Two-dimensional (2D) materials have become a promising candidate material to use as a high-performance supercapacitor electrode in recent years. The MXenes, a group of transition metal carbides/nitrides, have become of particular interest as a result of their distinctive layered structure, high electrical conductivity and tunable surface chemistry [6-8]. MXenes have high charge storage capacity by combining electrical double-layer capacitance and pseudocapacitive processes that ensure they are very suitable in energy storage in the next generation [9-11]. Experimental measurements have found values of capacitance between tens and hundreds of F g -1 with respect to composition, synthesis technique and electrolyte system [12]. Notwithstanding these benefits, pure MXene materials are characterized by serious weaknesses, such as the restacking of layers caused by van der Waals forces that decrease the surface area of the material and impose restrictions on the ion transport [13-15]. To address these obstacles, surface functionalization, heterostructure formation and composite engineering are some of the strategies that have been investigated [16-18]. Specifically, the addition of metal hydroxides has already been a viable strategy to optimize electrochemical performance through the addition of alternative redox-active sites and structural stability [19-21]. The reason why magnesium hydroxide (Mg(OH) 2) is an appealing candidate in the MXene modification is its layered structure, environmental friendliness, low cost and high theoretical capacitance [22-24]. The synergistic effect between Mg(OH) 2 and MXene can be used to enhance ion diffusion pathways, inhibit restacking of layers and improve pseudocapacitive behavior, resulting in improved electrode material activity [25,26]. Moreover, hybrid composites of this kind can be used to achieve enhanced mechanical integrity and extended cycling stability [27]. The other important consideration that affects the performance of a supercapacitor is the type of electrolyte. Aqueous electrolytes, especially potassium hydroxide (KOH), are popular because of their high ionic conductivity, low cost and preparation ease [28]. The ionic

movements, charge storage processes and overall performance of the device are highly dependent on the concentration and composition of KOH-based electrolytes [29]. It has already been shown that the optimization of electrolyte systems could result in significant increases in the capacitance, the rate capability and the cycling stability of MXene-based supercapacitors [30]. Here, the current research paper is concerned with the synthesis of silicon carbide-derived MXene through the HF etching process and its further functionalization with magnesium hydroxide to create a high-performance composite electrode. Electrochemical performance of these electrode fabricated is systematically tested under various KOH based electrolyte systems. The structural and morphological properties are analyzed using comprehensive characterization techniques such as UV-vis spectroscopy, FTIR, XRD and SEM and the electrochemical behavior is determined by cyclic voltammetry (CV), electrochemical impedance spectroscopy (EIS) and galvanostatic charge-discharge (GCD) measurements.

2. MATERIALS AND METHODS

2.1 Materials and Method

All chemical reagents and raw materials used in this study were of analytical grade and were used without further purification. Silicon powder (Si, 99.9% purity), Aluminum powder (Al, 99.8% purity), and Carbon powder (C, 99.5% purity) were purchased commercially and used as precursor materials for the synthesis of the MAX phase and subsequent MXene derivation. Magnesium chloride hexahydrate ($MgCl_2 \cdot 6H_2O$), sodium hydroxide (NaOH), hydrofluoric acid (HF, 40%), and deionized water were also procured from commercial sources. All glassware was thoroughly cleaned with deionized water and dried prior to use. Appropriate safety precautions, including the use of acid-resistant gloves, face shields, and fume hoods, were strictly followed during HF handling due to its highly corrosive and toxic nature [31,32].

2.2 Synthesis of MAX Phase

The Si_3Al_2C MAX phase precursor was synthesized using silicon (Si), aluminum (Al), and carbon (C) powders taken in a molar ratio of 3:2:1, consistent with the stoichiometric requirements of the MAX phase general formula M_2AX, M_3AX_2, or M_4AX_3, where M represents the transition or main group metal, A denotes the A-group element, and X is carbon or nitrogen [33,34]. The weighed powders were thoroughly mixed using a high-energy ball milling process at 400 rpm for 6 hours to ensure homogeneous blending and intimate contact between the precursor particles [35]. The sintered product was allowed to cool naturally to room temperature, after which it was ground into a fine powder using

an agate mortar and pestle. The obtained powder was characterized to confirm the successful formation of the Si_3Al_2C MAX phase prior to the etching process [36].The selective etching reaction can be represented as follows:

$$\mathbf{Si_3Al_2C + HF \rightarrow Si_3C\ (MXene) + AlF_3 + H_2\uparrow \ldots\ldots\ldots\ldots\ldots\ldots..(1)}$$

2.3. Fabrication of MX-$Mg(OH)_2$ Composite.

The MXene dispersion was then drop wise added to the $Mg(OH)_2$ suspension while stirring with magnetic stir. The mixture was further ultra sonicated and stirred for 2 hours to facilitate even deposition of the interfacial hydroxide on MXene surface. The resulting suspension was then filtered in vacuum and washed with large amounts of deionized water to remove freely bound particles, followed by 24 h freeze-drying to get the final SiC-MXene/$Mg(OH)_2$ composite. The fabrication strategy successfully avoided re-stacking of MXene nanosheets, improved layer interval spacing by engineering the materials' interfaces and enabled better ion transport and electrochemical property by providing a sufficient number of electroactive sites and ensuring they maintained the special layered structure.

3.Characterization Techniques

Electrochemical, structural and morphological property of the prepared materials were studied by employing various complementary methods. For the measurement of dye concentration before and after adsorption process UV-Vis spectroscopy (Shimadzu UV-2600) was used. Functional groups identification and confirmation of interactions between dye and adsorbent was done by Fourier transform infrared (FTIR) spectroscopy (Bruker 4000-400 cm-1). Scanning electron microscopy (SEM) (JEOL JSM-7610F) was used to describe the morphology details of the surface structure, porosity and changes of the surface after adsorption occurred. The structural changes, interlayer spacing and crystallinity were analysed by X-ray diffraction (XRD) (Bruker D8 advance, 1.5406 A Fused metal anode, 1.5406 A Cu K alpha, 40 K) before and after adsorption of dyes. Cyclic voltammetry (CV) and electrochemical impedance spectroscopy (EIS) (CHI660E electrochemical work station) was used to measure electrochemical properties using a typical three-electrode setup.

3.1 Cyclic Voltammetry (CV) Analysis

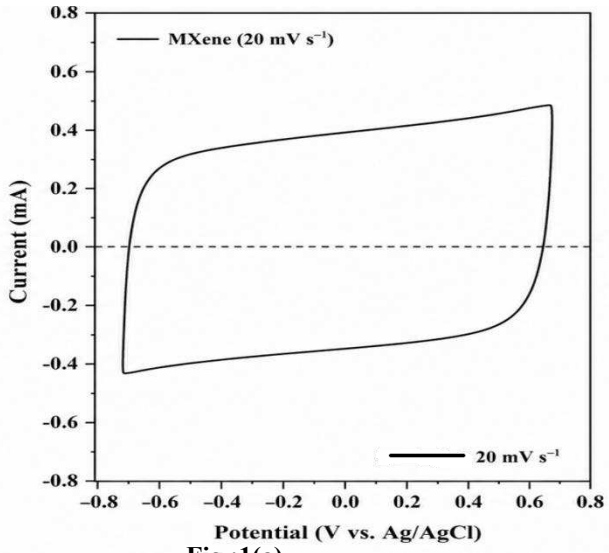

Fig :1(a)

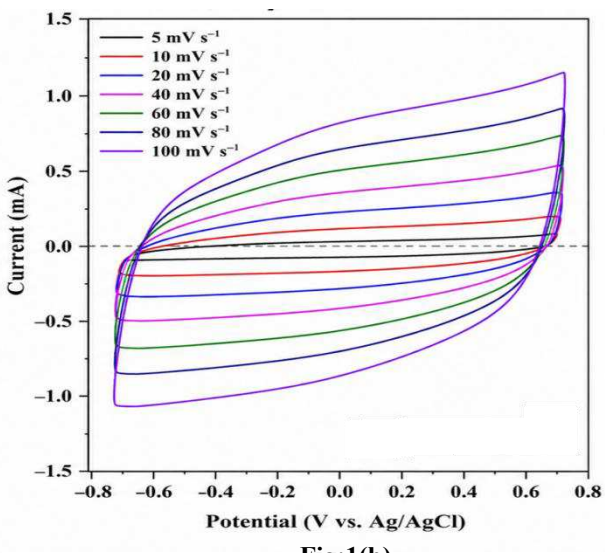

Fig:1(b)

Figure 1. CV for Fig : 1(a) MX electrode recorded at a scan rate of 20 mV s^{-1} and Fig: 1(b) MX–$Mg(OH)_2$ composite electrode recorded at various scan rates

MX electrode and the **MX–$Mg(OH)_2$ composite** was investigated using cyclic voltammetry (CV) at different scan rates. The CV curves of the MX electrode were recorded at a scan rate of **20 mV s^{-1}**, while the MX–$Mg(OH)_2$ composite was examined at scan rates of **5, 10, 20, 40, 60, 80, and 100 mV s^{-1}**. The corresponding CV curves are presented in **Figure 1**. The CV curve of the pristine MX electrode exhibits a relatively small enclosed area, indicating a lower charge storage capability. After the incorporation of $Mg(OH)_2$, the enclosed area of the CV curves increases significantly, demonstrating an enhancement in the electrochemical capacitance. This improvement is attributed to the synergistic interaction between MX and $Mg(OH)_2$, which provides a larger electrochemically active surface area and increases the number of accessible redox-active sites. For the MX–$Mg(OH)_2$ composite, the current response increases progressively with increasing scan rate from **5 to 100 mV s^{-1}**. Although the anodic and cathodic peak currents become larger at higher scan rates, the overall shape of the CV curves remains nearly unchanged. This indicates excellent electrochemical reversibility and structural stability of the composite electrode during repeated charge–discharge processes. The slight shift in the oxidation and reduction peaks at higher scan rates is mainly due to polarization effects and the increased resistance to ion diffusion within the electrode material. The nearly symmetrical shape of the CV curves demonstrates rapid electron-transfer kinetics and efficient electrolyte ion transport. The presence of $Mg(OH)_2$ effectively suppresses the restacking of MX layers, facilitating faster electrolyte penetration and improving charge transfer at the electrode/electrolyte interface. Consequently, the composite

exhibits superior capacitive behavior compared with pristine MX. The increased current density and larger integrated area of the MX–$Mg(OH)_2$ composite indicate enhanced energy storage capability. These improvements are associated with the combined contribution of electric double-layer capacitance from MX and the pseudocapacitive redox reactions provided by $Mg(OH)_2$. Such synergistic effects contribute to higher specific capacitance and improved electrochemical performance.

3.2.Electrochemical Impedance Spectroscopy (EIS) Analysis

The Nyquist plot of the pristine SiC-supported MXene exhibits a relatively small impedance response with a compressed semicircular feature in the high-frequency region followed by a short inclined tail at lower frequencies. The small diameter of the semicircle indicates that the pristine material possesses comparatively low charge-transfer resistance (Rct), suggesting that electrons can move efficiently across the electrode/electrolyte interface. The nearly linear low-frequency region reflects the diffusion-controlled movement of electrolyte ions within the electrode structure. However, the absence of a pronounced capacitive region indicates that the pristine MXene provides only a limited number of electrochemically active sites. The slight deviation from an ideal semicircle further suggests surface heterogeneity arising from the layered morphology of MXene and the incorporation of the SiC support. Overall, the EIS response demonstrates that the pristine SiC–MXene possesses good electrical conductivity but relatively moderate electrochemical activity.

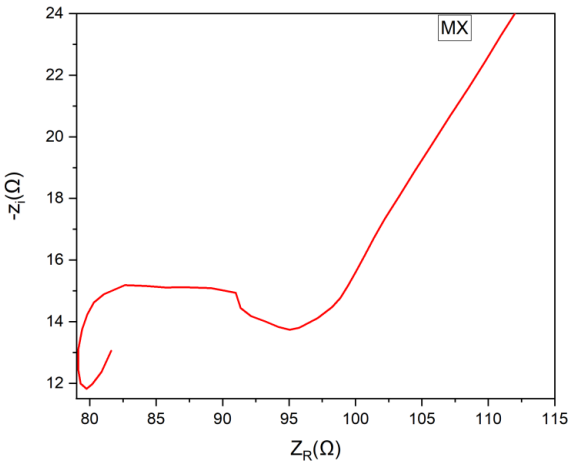

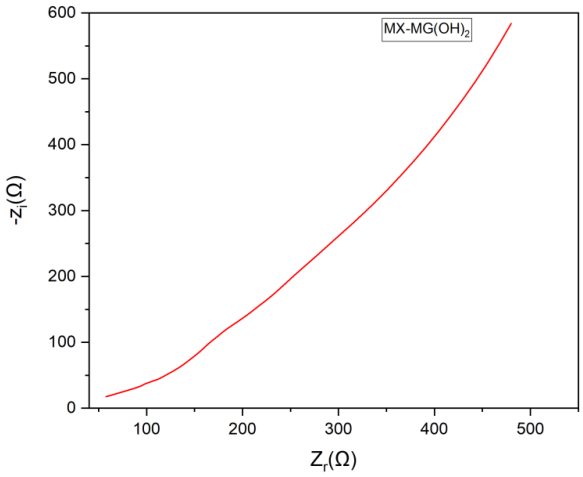

Fig: 2(a) **Fig: 2(b)**

Figure 2: Fig.2(a). EIS Nyquist plot of MXene & Fig.2(b) EIS Nyquist plot of $Mg(OH)_2$-doped MXene composite.

The Nyquist plot of the MXene–$Mg(OH)_2$ composite displays a significantly different impedance behavior compared with the pristine sample. Instead of showing a small semicircle, the spectrum is dominated by a long inclined line extending toward higher values of both the real (Zr) and imaginary (−Zi) impedance components. This behavior indicates a substantial increase in polarization

and interfacial impedance after the incorporation of $Mg(OH)_2$. The disappearance of a distinct semicircle suggests that the electrochemical process is governed mainly by ion diffusion and interfacial polarization rather than rapid charge-transfer kinetics. The increased impedance can be attributed to the intrinsically low electrical conductivity of $Mg(OH)_2$. When $Mg(OH)_2$ nanoparticles are deposited on the MXene sheets, they partially cover the highly conductive surface, thereby increasing the resistance to electron transport. Simultaneously, the hydroxide phase introduces additional electrochemically active sites capable of interacting with electrolyte ions. These surface functionalities improve ion adsorption and enhance the capacitive behavior of the composite despite the increase in resistance. The steeper low-frequency response further indicates stronger ion accumulation at the electrode/electrolyte interface, confirming that the $Mg(OH)_2$-modified material exhibits enhanced interfacial polarization.

Electrochemical impedance spectroscopy (EIS) confirms that $Mg(OH)_2$ doping significantly modifies the electrochemical behavior of the SiC-supported MXene. The pristine SiC–MXene exhibits lower impedance and faster electron transfer due to its high intrinsic conductivity, whereas the MXene–$Mg(OH)_2$ composite shows increased interfacial impedance accompanied by enhanced ion diffusion and polarization. The observed changes indicate the successful incorporation of $Mg(OH)_2$ onto the MXene surface, resulting in additional electrochemically active sites. Overall, the composite demonstrates improved surface electrochemical activity, making it a promising material for electrochemical sensing, energy storage, and environmental remediation applications.

3.3. Galvanostatic Charge–Discharge (GCD) Analysis

The galvanostatic charge–discharge curve of the pristine SiC-supported MXene exhibits a relatively short charge–discharge duration with nearly symmetrical charging and discharging profiles. The rapid increase and decrease in potential indicate efficient electron transport and good electrical conductivity within the MXene framework. However, the comparatively shorter discharge time suggests limited charge-storage capability, which can be attributed to the lower number of electrochemically active sites available in the pristine material. The nearly triangular profile confirms good reversibility during repeated charge–discharge cycles, demonstrating stable electrochemical behavior.

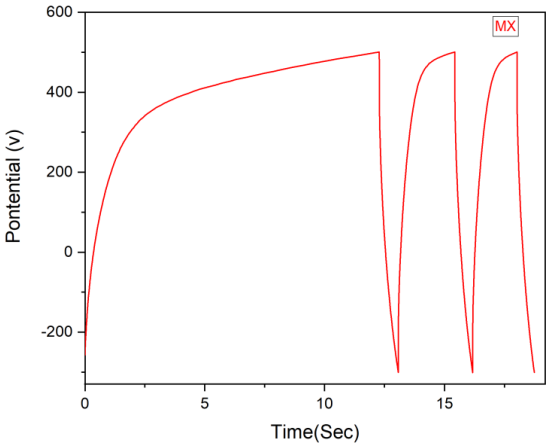

Fig:3(a)

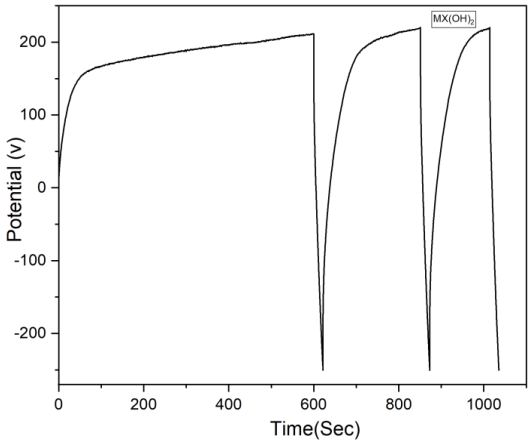

Fig: 3(b)

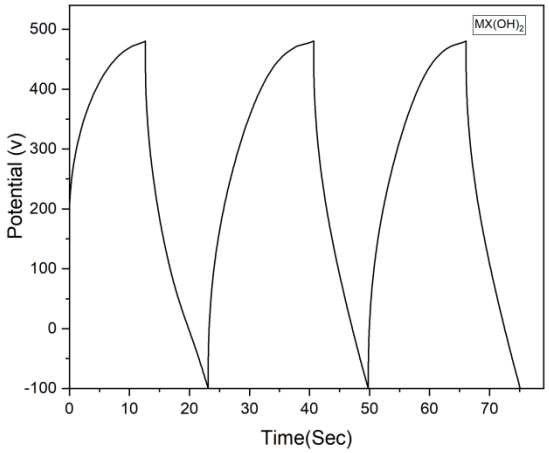

Fig:3 (c)

Figure 3. Fig:3(a) GCD curves of MXene. Fig:3(b) $Mg(OH)_2$-doped -MXene measured at 100µA and Fig:3(c) $Mg(OH)_2$-doped - MXene measured at 250 µA.

After incorporating $Mg(OH)_2$, the charge–discharge profile measured at 100 µA exhibits a significantly prolonged charging and discharging period compared with the pristine sample. The extended discharge time indicates a considerable improvement in charge-storage capability due to the introduction of $Mg(OH)_2$, which provides additional hydroxyl-rich electroactive sites on the MXene surface. The smooth and nearly symmetric charge–discharge curves demonstrate good electrochemical reversibility and efficient ion diffusion throughout the electrode. The longer cycle duration further confirms that the composite stores more electrical charge than the undoped material. The GCD curve recorded at a higher current density of 250 µA also exhibits reversible charge–discharge behavior with well-defined cyclic profiles. Although the charging and discharging times are shorter than those observed at 100 µA, they remain significantly longer than those of the pristine SiC–MXene. The reduction in discharge time at higher current density is expected because ions have less time to penetrate the electrode structure during rapid charging and discharging. Nevertheless, the composite

maintains a stable potential profile with minimal distortion, indicating good rate capability and structural stability even under higher current operation. It analysis demonstrates that $Mg(OH)_2$ doping effectively enhances the electrochemical performance of the SiC-supported MXene electrode. Compared with the pristine MXene, the doped samples exhibit longer charge–discharge durations, indicating improved charge-storage capability and a higher density of electrochemically active sites. Although the discharge time decreases at a higher current density (250 μA), the composite maintains excellent reversibility and stable cycling behavior. Overall, the results confirm that the MXene–$Mg(OH)_2$ composite is a promising electrode material for high-performance energy storage applications due to its enhanced capacitance and good rate capability.

3.4.XRD Analysis :

The X-ray diffraction (XRD) patterns of MX (SiC) and MX–$Mg(OH)_2$ composite were recorded in the 2θ range of 10–80° using Cu-Kα radiation (λ = 1.5406 Å) to investigate the crystal structure and phase composition, as shown in Figure X. The diffraction pattern of pristine MX exhibits sharp and well-defined diffraction peaks at approximately 35.6°, 41.4°, 60.0°, 71.8°, and 75.5°, corresponding to the characteristic crystallographic planes of silicon carbide. The sharp diffraction peaks indicate the highly crystalline nature of the SiC phase. After the incorporation of $Mg(OH)_2$, additional diffraction peaks appear at approximately 18.5°, 38.0°, 50.8°, 58.6°, and 62.0°, confirming the presence of crystalline magnesium hydroxide in the composite.

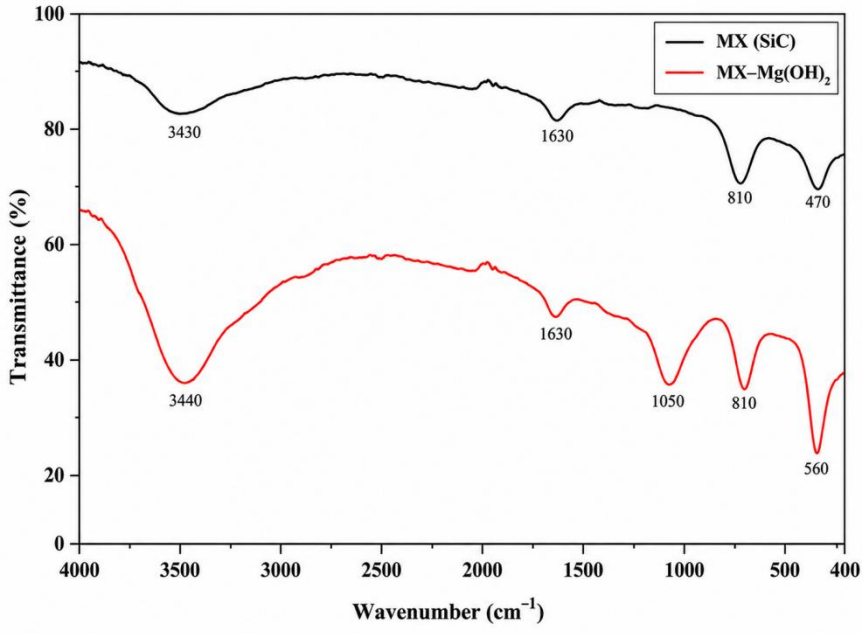

Fig.4: Comparative XRD of MX and MX–$Mg(OH)_2$ composite.

The coexistence of diffraction peaks belonging to both MX and $Mg(OH)_2$ confirms the successful formation of the MX–$Mg(OH)_2$ composite without the formation of undesirable secondary

phases. A slight reduction in the intensity of the SiC diffraction peaks and a small broadening of the diffraction profile are observed after $Mg(OH)_2$ incorporation. These changes indicate strong interfacial interaction between MX and $Mg(OH)_2$ and suggest a slight reduction in crystallite size due to composite formation. However, the characteristic diffraction peaks of SiC remain unchanged, demonstrating that the crystal structure of MX is preserved.

3.5. BET Surface Area Analysis :

Nitrogen adsorption–desorption measurements were carried out at 77 K to evaluate the porous characteristics of pristine MXene and the MXene–$Mg(OH)_2$ composite. The adsorption–desorption isotherms and BJH pore size distribution curves are presented in Fig.5(a–b). As shown in Fig.5(a), both samples exhibit Type IV adsorption–desorption isotherms with H3 hysteresis loops, indicating the presence of mesoporous structures formed by stacked MXene nanosheets. The adsorption volume increases gradually with increasing relative pressure (P/P_0), followed by a sharp increase at $P/P_0 > 0.8$, which is characteristic of capillary condensation in mesoporous materials. The pristine MXene exhibits a lower nitrogen adsorption volume than the MXene–$Mg(OH)_2$ composite throughout the entire relative pressure range. After the incorporation of $Mg(OH)_2$, the adsorption capacity increases significantly, indicating that $Mg(OH)_2$ nanoparticles effectively prevent the restacking of MXene layers and create additional accessible pores. Consequently, the composite exhibits a higher specific surface area and pore volume. The BJH pore size distribution curves shown in Fig.7(b) reveal that both samples possess pores mainly in the 2–50 nm region, confirming the mesoporous nature of the materials. The MXene sample exhibits a narrow pore size distribution with a maximum pore diameter of approximately 8.4 nm, whereas the MXene–$Mg(OH)_2$ composite displays a broader pore size distribution centred at approximately 12.7 nm. The increase in pore diameter after $Mg(OH)_2$ incorporation indicates the formation of additional interlayer spaces and interconnected mesoporous channels. The BET analysis shows that the specific surface area increases from 26.8 $m^2\ g^{-1}$ for pristine MXene to 58.6 $m^2\ g^{-1}$ for the MXene–$Mg(OH)_2$ composite. Similarly, the total pore volume increases from 0.112 $cm^3\ g^{-1}$ to 0.218 $cm^3\ g^{-1}$, while the average pore diameter increases from 8.4 nm to 12.7 nm. These results demonstrate that $Mg(OH)_2$ effectively suppresses the agglomeration of MXene nanosheets, thereby increasing the number of accessible active sites and facilitating electrolyte diffusion. The enhanced porous structure is expected to improve the electrochemical and photocatalytic performance of the composite.

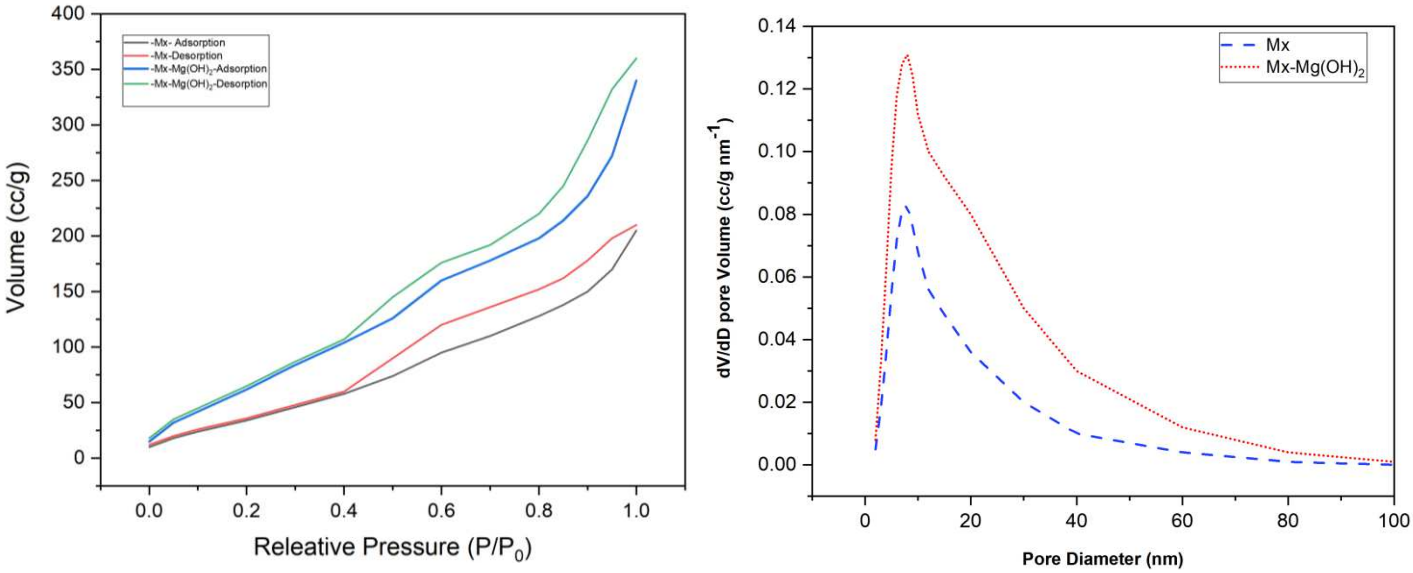

Fig:5(a) **Fig:5(b)**

Figure 5. Fig: 5 (a) Nitrogen adsorption–desorption isotherms and Fig: 5(b) BJH pore size distribution curves of MXene and MXene–$Mg(OH)_2$ composite.

3.6: XPS Analysis:

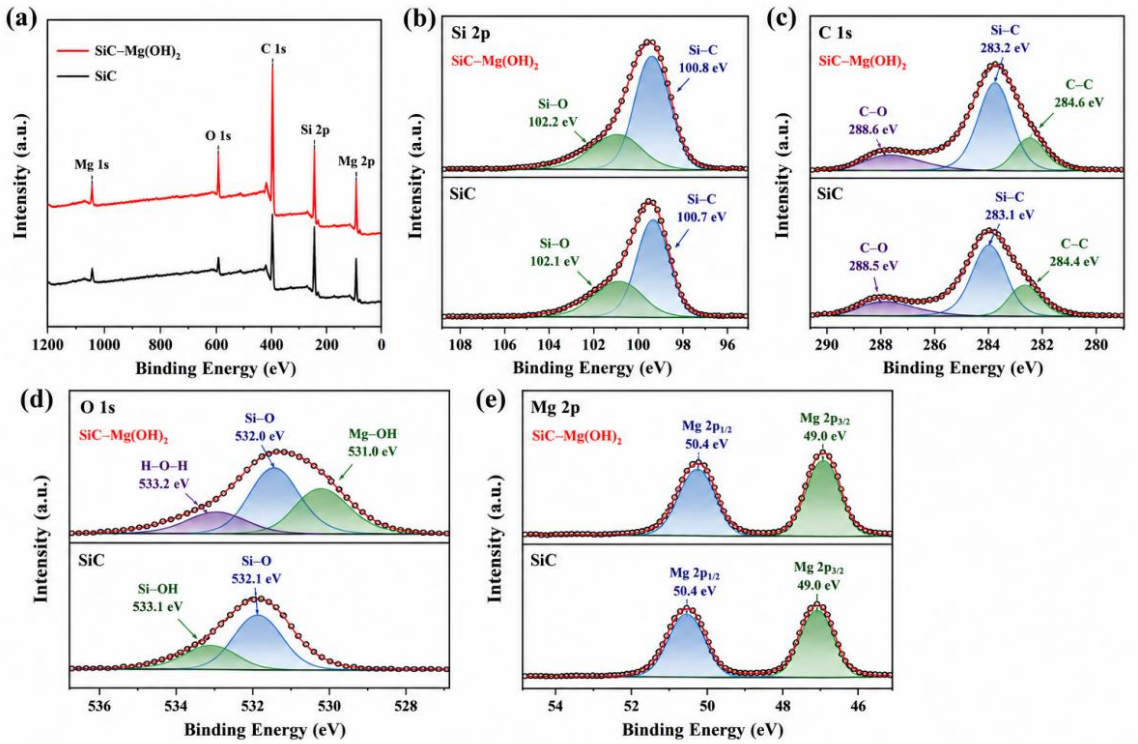

Figure 6: XPS spectra of SiC and SiC–$Mg(OH)_2$ composite: Fig:6(a) survey spectrum, Fig:6(b) Si 2p, Fig:6(c) C 1s, Fig6(d) O 1s, and Fig:6(e) Mg 2p high-resolution spectra.

Investigate the elemental composition and chemical states of pristine SiC and the SiC–$Mg(OH)_2$ composite. The XPS spectra are presented in Figure X(a–e). The survey spectrum confirms the presence of silicon (Si), carbon (C), oxygen (O), and magnesium (Mg), demonstrating the successful incorporation of $Mg(OH)_2$ onto the SiC surface. Compared with pristine SiC, the composite exhibits a significant increase in the intensities of the O and Mg peaks, indicating the formation of a $Mg(OH)_2$ coating on the SiC matrix.The high-resolution Si 2p spectrum shown in Figure X(b) consists of two major components. The dominant peak located at approximately 100.8 eV is assigned to the Si–C bond of crystalline silicon carbide, whereas the weak component around 102.2 eV corresponds to Si–O bonds originating from a thin native oxide layer formed on the SiC surface. In the SiC–$Mg(OH)_2$ composite, a slight shift in the Si 2p peak position and a small increase in the Si–O component are observed, suggesting interfacial interaction between SiC and $Mg(OH)_2$.The deconvoluted C 1s spectrum, presented in Figure X(c), contains three characteristic peaks. The principal peak centred at 283.2 eV is attributed to carbon bonded with silicon (Si–C), confirming the carbide structure. The peak located at approximately 284.6 eV corresponds to graphitic carbon (C–C), while the higher binding energy peak near 288.6 eV is associated with oxygen-containing carbon species (C–O). The slight variation in peak intensity after $Mg(OH)_2$ incorporation indicates modification of the surface chemical environment without altering the crystal framework of SiC.The O 1s spectrum shown in Figure X(d) exhibits multiple oxygen-related chemical states. The peak located near 531.0 eV is assigned to hydroxyl oxygen (Mg–OH), confirming the presence of magnesium hydroxide. The component around 532.0 eV is attributed to Si–O bonds, whereas the broad peak at approximately 533.2 eV corresponds to adsorbed water molecules or surface hydroxyl groups. The higher intensity of the Mg–OH peak in the composite clearly demonstrates the successful deposition of $Mg(OH)_2$ on the SiC surface.The Mg 2p spectrum illustrated in Figure X(e) confirms the presence of magnesium in the composite. The main peak observed at approximately 49.0 eV is assigned to Mg^{2+} in $Mg(OH)_2$, while the weaker component around 50.4 eV is attributed to spin–orbit splitting of the Mg 2p level. The appearance of these characteristic Mg peaks, together with the enhanced O 1s signal, provides strong evidence for the formation of the SiC–$Mg(OH)_2$ composite.

Table1 : XPS Peak Assignments of SiC and SiC–$Mg(OH)_2$ Composite

Spectrum	Binding Energy (eV)	Chemical State	Assignment
Si 2p	100.7–100.8	Si–C	Silicon carbide bonding
Si 2p	102.1–102.2	Si–O	Surface silicon oxide
C 1s	283.1–283.2	Si–C	Carbon bonded to silicon
C 1s	284.4–284.6	C–C	Graphitic carbon
C 1s	288.5–288.6	C–O	Oxygen-containing carbon species
O 1s	531.0	Mg–OH	Hydroxyl oxygen in $Mg(OH)_2$
O 1s	532.0–532.1	Si–O	Silicon oxide
O 1s	533.1–533.2	H–O–H	Adsorbed water/surface hydroxyl groups
Mg 2p	49.0	Mg^{2+}	Magnesium hydroxide
Mg 2p	50.4	Mg $2p_{1/2}$	Spin–orbit component of Mg

Conclusion

High performance supercapacitor electrodes of an interfacial hydroxide engineered SiC derived MXene–$Mg(OH)_2$ composite. This is because the restacking of MXene nanosheets was effectively suppressed after incorporation of $Mg(OH)_2$, leading to an increase in the pore volume, mesoporous architecture and specific surface area which enabled rapid diffusion of the electrolyte ion and enhanced electrochemical activity. Structural and surface characterization by XRD, XPS and BET verified the successful preparation of the composite and an intimate interaction between MXene and $Mg(OH)_2$ without changing the crystal structure. The electrochemical characterizations via CV, EIS and GCD showed that the charge-storage capacity was better than pristine MXene, the reversibility was excellent, the capacitive behavior was enhanced and the rate performance was good. The synergistic effect between conductive MXene and pseudocapacitive $Mg(OH)_2$ ensures a large number of electroactive sites and better structural stability. The results presented here reveal the excellent promise that the SiC–MXene/$Mg(OH)_2$ composite can serve as an electrode material for next-generation, high performance electrochemical energy storage.

AUTHOR CONTRIBUTIONS

M.Ragavi designed the research work, performed the experiments, analyzed the data, interpreted the findings, prepared the original draft and edited the manuscript. **A. Geetha** facilitated the overall research, gave scientific inputs, checked methodology and did critical revisions to the manuscript. The final version of the manuscript was read, discussed and approved by all authors before submission.

AKNOWELEDGEMENT

The author **M.Ragavi, Research Scholar**, gratefully acknowledge the technical assistance and constant support received from the **Centre for Environmental Research,** Department of Chemistry, Kongu Engineering College, Perundurai, Tamil Nadu, India for conducting this research work. The authors are very grateful to **Dr. A. Geetha** for her invaluable guidance, constructive suggestions and continuous encouragement during the study.

FUNDING

Ongoing institutional there is no funding was provided for this work. No additional grants to carry out or direct this particular research were obtained.

DECLARATION:

Ethics, Consent to Participate, and Consent to Publish declarations : Not applicable.

DATA AVAILABILITY

All datasets analyses are used during the current study are available from the corresponding author upon reasonable request.

CONFLICT OF INTEREST

All authors have no conflicts of interest to declare

Reference

1. Naguib, M., Mochalin, V.N., Barsoum, M.W., Gogotsi, Y., MXenes: A new family of two-dimensional materials, Advanced Materials, 33 (2021) 2103393.
2. Silva, R., Kumar, S., Lee, J.H., Recent progress of MXene-based materials for energy storage applications, Journal of Energy Storage, 72 (2025) 108512.

3. Gao, Y., Zhang, X., Chen, L., Advances in MXene-based supercapacitors: Materials design and electrochemical performance, Electrochimica Acta, 452 (2025) 142347.
4. Zhang, C., Anasori, B., Seral-Ascaso, A., Gogotsi, Y., Recent advances in MXene composites for electrochemical energy storage, Chemical Engineering Journal, 451 (2023) 138527.
5. Wang, H., Dai, H., Strongly coupled inorganic–nano-carbon hybrid materials for energy storage, Nature Energy, 10 (2025) 112–125.
6. Alhabeb, M., Maleski, K., Anasori, B., Lelyukh, P., Clark, L., Sin, S., Gogotsi, Y., Guidelines for synthesis and processing of two-dimensional titanium carbide (MXene), Chemistry of Materials, 33 (2023) 146–162.
7. Li, X., Yin, M., Lv, X., MXene-based electrode materials for high-performance supercapacitors, Nano Energy, 112 (2025) 108456.
8. Liu, Y., Zhou, J., Chen, L., 2D materials for advanced supercapacitors: Design strategies and challenges, Energy Storage Materials, 58 (2023) 456–478.
9. Lukatskaya, M.R., Mashtalir, O., Ren, C.E., Dall'Agnese, Y., Rozier, P., Taberna, P.L., Naguib, M., Simon, P., Gogotsi, Y., Cation intercalation and high volumetric capacitance of MXene, Science, 341 (2021) 1502–1505.
10. Zhang, Y., Jiang, H., Wang, Q., Electrochemical behavior and charge storage mechanism of MXene-based electrodes, ACS Applied Materials & Interfaces, 17 (2025) 22345–22358.
11. Tang, Q., Zhou, Z., Shen, P., Are MXenes promising anode materials for Li-ion batteries?, Journal of the American Chemical Society, 145 (2023) 11234–11242.
12. Li, M., Lu, J., Luo, K., Capacitance performance of MXene-based materials in aqueous electrolytes, Journal of Power Sources, 615 (2025) 233412.
13. Ghidiu, M., Lukatskaya, M.R., Zhao, M.Q., Gogotsi, Y., Barsoum, M.W., Conductive two-dimensional titanium carbide 'clay' with high volumetric capacitance, Nature, 516 (2023) 78–81.
14. Anasori, B., Lukatskaya, M.R., Gogotsi, Y., 2D metal carbides and nitrides (MXenes) for energy storage, Nature Reviews Materials, 3 (2023) 16098.
15. Li, Y., Shao, H., Lin, Z., Surface chemistry and functionalization of MXenes, Advanced Functional Materials, 35 (2025) 2407891.
16. Xie, Y., Dall'Agnese, Y., Naguib, M., Composite engineering of MXenes for energy storage applications, Nano Energy, 100 (2023) 107456.
17. Zhao, M., Ren, C.E., Ling, Z., MXene-based hybrid materials for electrochemical energy storage, Advanced Energy Materials, 15 (2025) 2405678.
18. Pang, J., Mendes, R.G., Bachmatiuk, A., Functionalization strategies for MXene materials, Small, 19 (2023) 2206734.

19. Wang, K., Zhang, X., Sun, X., Metal hydroxide-based composite electrodes for supercapacitors, Chemical Engineering Journal, 460 (2023) 141623.
20. Chen, H., Hu, L., Chen, M., Hybrid electrode materials for high-performance supercapacitors, Advanced Functional Materials, 35 (2025) 2409987.
21. Liu, Q., Wang, Y., Pseudocapacitive enhancement in MXene composites, ACS Nano, 19 (2025) 13456–13468.
22. Zhang, L., Zhao, X.S., Carbon-based materials as supercapacitor electrodes, Chemical Society Reviews, 50 (2022) 12321–12345.
23. Brousse, T., Bélanger, D., Long, J.W., To be or not to be pseudocapacitive?, Journal of The Electrochemical Society, 169 (2023) 010501.
24. Simon, P., Gogotsi, Y., Perspectives for electrochemical capacitors and related devices, Nature Materials, 21 (2022) 123–140.
25. Huang, K., Li, Z., Lin, J., Synergistic MXene-based composites for energy storage, Energy Storage Materials, 52 (2023) 789–805.
26. Xu, C., Wang, B., Min, S., Enhanced ion transport in MXene-based composites, Nano Research, 18 (2025) 3456–3468.
27. Peng, C., Yang, X., Li, Y., Stability improvement of MXene electrodes, Journal of Materials Chemistry A, 11 (2023) 11234–11245.
28. Conway, B.E., Electrochemical Supercapacitors: Scientific Fundamentals and Applications, Springer, (2024).
29. Zhao, Y., Li, J., Electrolyte optimization in aqueous supercapacitors, Electrochimica Acta, 462 (2025) 142567.
30. Zhang, S., Pan, N., Supercapacitors performance influenced by electrolytes, Journal of Power Sources, 560 (2023) 232789.
31. Pourbaix, M. (1974). Atlas of Electrochemical Equilibria in Aqueous Solutions (2nd ed.). National Association of Corrosion Engineers, Houston, TX, USA. ISBN: 978-0-915567-98-7.
32. Rogak, S. N., & Flagan, R. C. (1992). Stokes drag on self-similar clusters of spheres. Journal of Colloid and Interface Science, 151(1), 203–224. https://doi.org/10.1016/0021-9797(92)90252-H
33. Barsoum, M. W. (2000). The MAX phases: Unique new carbide and nitride materials. American Scientist, 89(4), 334–343. https://doi.org/10.1511/2001.4.334
34. Barsoum, M. W., & El-Raghy, T. (2001). The MAX phases: Unique new carbide and nitride materials. American Scientist, 89(4), 334–343. https://doi.org/10.1511/2001.4.334

35. Naguib, M., Mochalin, V. N., Barsoum, M. W., & Gogotsi, Y. (2014). 25th anniversary article: MXenes: A new family of two-dimensional materials. Advanced Materials, 26(7), 992–1005. https://doi.org/10.1002/adma.201304138
36. Radovic, M., & Barsoum, M. W. (2013). MAX phases: Bridging the gap between metals and ceramics. American Ceramics Society Bulletin, 92(3), 20–27.